# Weakening Trend in the Atmospheric Heat Source over the Tibetan Plateau during Recent Decades. Part I: Observations

ANMIN DUAN AND GUOXIONG WU

*State Key Laboratory of Numerical Modelling for Atmospheric Sciences and Geophysical Fluid Dynamics, Institute of Atmospheric Physics, Chinese Academy of Sciences, Beijing, China*

(Manuscript received 23 February 2007, in final form 13 November 2007)

ABSTRACT

The trend in the atmospheric heat source over the Tibetan Plateau (TP) during the last four decades is evaluated using historical observations at 74 meteorological stations in the period of 1961–2003 and satellite radiation data from 1983 to 2004. It is shown that in contrast to the strong surface and troposphere warming, the sensible heat (SH) flux over the TP exhibits a significant decreasing trend since the mid-1980s. The largest trend occurs in spring, a season of the highest SH over the TP. The subdued surface wind speed contributes most to the decreasing trend. At the same time, the radiative cooling effect in the air column enhances persistently. Despite the fact that the in situ latent heating presents a weak increasing trend, the springtime atmospheric heat source over the TP loses its strength during two recent decades. Further investigation suggests that the weakened SH over the TP may be part of the global circulation shift.

## 1. Introduction

The Tibetan Plateau (TP) is located in the subtropical central and eastern Eurasian continent, acting as a huge, intense, and elevated heat source with strong sensible heating (SH) in the surface layers. The mechanical and thermal forcing of the TP plays a crucial role not only in the onset and maintenance of the Asian summer monsoon (e.g., Yeh et al. 1957; Flohn 1957, 1960; Yanai et al. 1992; Li and Yanai 1996; Li et al. 2001; Zhao and Chen 2001; Kitoh 2004; Yanai and Wu 2006; Wu et al. 2007), but also in the development of weather systems over east China (Tao and Ding 1981) and even the boreal summer climate pattern (Hahn and Manabe 1975; Broccoli and Manabe 1992; Duan and Wu 2005, hereafter DW05).

Growing evidence has shown that a striking climate warming occurred over the TP during the second half of the twentieth century (e.g., Liu and Chen 2000; Zhu et al. 2001; Niu et al. 2004). Most recent analysis indicates that the increased surface air temperature was accompanied by a diminished diurnal range in surface air temperature, a warmed troposphere, and a cooled lower stratosphere (Duan et al. 2006). The decrease of the in situ cloud amount and the accompanied change of radiation process are important for the increase of surface air temperature and the diminished diurnal range (Duan and Wu 2006, hereafter DW06). Moreover, numerical simulation results given by both regional and global climate models further suggest that the recent climate warming over the TP is likely to be induced by the enhanced anthropogenic greenhouse gases effect (Chen et al. 2003; Duan et al. 2006).

The climate warming over the TP should be accompanied by a change in the atmospheric heat source, not only its intensity, but also its diurnal variation and seasonal evolution. Zhang et al. (2004) found that the snow depth over the TP exhibits a sharp increase during spring (March and April) after the 1970s, which implies excessive precipitation and land surface cooling. Similar results have also been obtained by a more recent study (Y. Zhu and Y. Ding 2006, personal communication), which hypothesized that there be a suppressed atmospheric heat source over the TP in spring. So far, however, there has not been any investigation concerning the decadal change of the heat source over the TP and its possible connection with the global circulation shift. The main objectives of this study, therefore, are to determine quantitatively the long-term trend in the atmospheric heat source over the TP and to

*Corresponding author address:* Anmin Duan, State Key Laboratory of Numerical Modelling for Atmospheric Sciences and Geophysical Fluid Dynamics, Institute of Atmospheric Physics, Chinese Academy of Sciences, Beijing 100029, China.
E-mail: amduan@lasg.iap.ac.cn

DOI: 10.1175/2007JCLI1912.1

identify its possible connection with the global circulation shift.

The structure of this paper is as follows. The data and analysis procedures used in this study are described briefly in section 2. Section 3 introduces the climatology of the atmospheric heat source/sink over the TP, and section 4 describes the change of SH over the central and eastern TP (CE-TP) and over the western TP (W-TP). In section 5, decadal trends of the latent heating and radiative cooling are investigated to give an overall picture of the change in the atmospheric heating status over the TP. The relationship between the diabatic heating over the TP and the global climate change in decadal time scale is assessed in section 6, followed by conclusions and discussions in section 7.

## 2. Data and methodology

### a. Data

The data used in this study include the following sources:

1) The regular surface meteorological observations with an initial quality control for the TP region provided by the China Meteorological Administration (CMA). Variables are collected four times daily (0000, 0600, 1200, and 1800 LST at 90°E Lhasa time, 6 h earlier than UTC) and include surface air temperature ($T_a$), ground surface temperature ($T_s$), wind speed at 10 m above the surface ($V_0$), station surface pressure ($P_s$), and daily accumulative precipitation ($P_r$). We only analyze the data from 1961 to 2003 because most of the plateau meteorological observatories do not have continuous data until the 1960s.
2) Monthly records of the 12 radiosonde stations in the TP from 1980 to 2004 archived by CMA. They are monthly-mean air temperature, wind speed, and geopotential height at 16 standard pressure levels (1000, 925, 850, 700, 500, 400, 300, 250, 200, 150, 100, 70, 50, 30, 20, and 10 hPa). Since the height of the TP is almost at 600 hPa and balloons frequently burst over 10 hPa, the levels selected for the present study are limited to those from 500 to 20 hPa. Previous studies have shown that the quality of the radiosonde data in China is generally quite good (Wang and Ren 2005; Zhou and Zhang 2005).
3) The International Satellite Cloud Climatology Project (ISCCP, additional information is available online at http://isccp.giss.nasa.gov/projects/flux.html; Rossow and Schiffer 1991; 1999) radiation data are also utilized. Radiation fluxes include the downward and upward shortwave and longwave radiation fluxes at the top of the atmosphere and on the ground. The data period is from July 1983 to June 2005, with a horizontal resolution of 2.5° by 2.5°.

The locations and elevations of the stations are given in Fig. 1a, with more detailed information presented in the appendix. The highest and lowest stations are Bange (31.38°N, 90.02°E; 4700 m above sea level) and Zhaojue (28°N, 102.85°E; 2132 m), respectively. Minxian (34.43°N, 104.01°E; 2315 m), Dingri (28.63°N, 87.08°E; 4300 m), Huapin (26.63°N, 101.27°E; 2245 m), and Tuole (38.80°N, 98.42°E; 3367 m) outline the east, west, south, and north borders of the CE-TP area. Most of these stations are located in Qinghai and Xizang (Tibet) areas in China, and a few from the adjacent areas in Gansu, Sichuan, and Yunnan Provinces of China.

The data coverage is adequate to depict the trend in the domain except for the western plateau where there are only three stations: Shiquanhe (80.08°E, 32.50°N; 4278 m) founded in 1960, Gaize (84.42°E, 32.15°N; 4415 m) founded in 1973, and Pulan (81.25°E, 30.28°N; 3900 m) founded in 1973. Hence this study focuses mainly on the change of the atmospheric heat source in the CE-TP. The area averages over the CE-TP (26°–39°N, 85°–105°E) and W-TP (30°–33°N, 80°–85°E) are obtained using 54 and 6 grid points when the ISCCP data are used, as indicated by the two rectangular boxes in Fig. 1a.

As the first step of the data analysis, the missing data are filled by averaging the values of the previous year and the following year at the same time. This operation is done only once for every missing value. When there are still insufficient data after this, the missing value is replaced by its corresponding mean value at the same station. The missing $T_a$, $V_0$, and $P_r$ account for less than 0.5% of the total records, hence the quality of $T_a$, $V_0$, and $P_r$ is reasonably good. Missing $T_s$ is close to 8% of the total record, and most occurs before 1980s. To ensure a reliable outcome, the observations that suffer from such missing $T_s$ records are not included in the statistics before 1980, and only 37 observatories in the period 1961–2003 and 71 observatories in 1980–2003 are chosen for this study.

### b. Analysis procedures

Atmospheric heat source/sink ($E$) is a physical quantity used to discuss the heat budget in an air column. For a given location, an atmospheric heat source (sink) is defined when there is a net heat gain (loss) within a given period. The expression of $E$ is therefore defined as

$$E = \mathrm{SH} + \mathrm{LH} + \mathrm{RC}, \quad (1)$$

where SH denotes the local surface sensible heat transfer, LH is the latent heat released to the atmosphere by

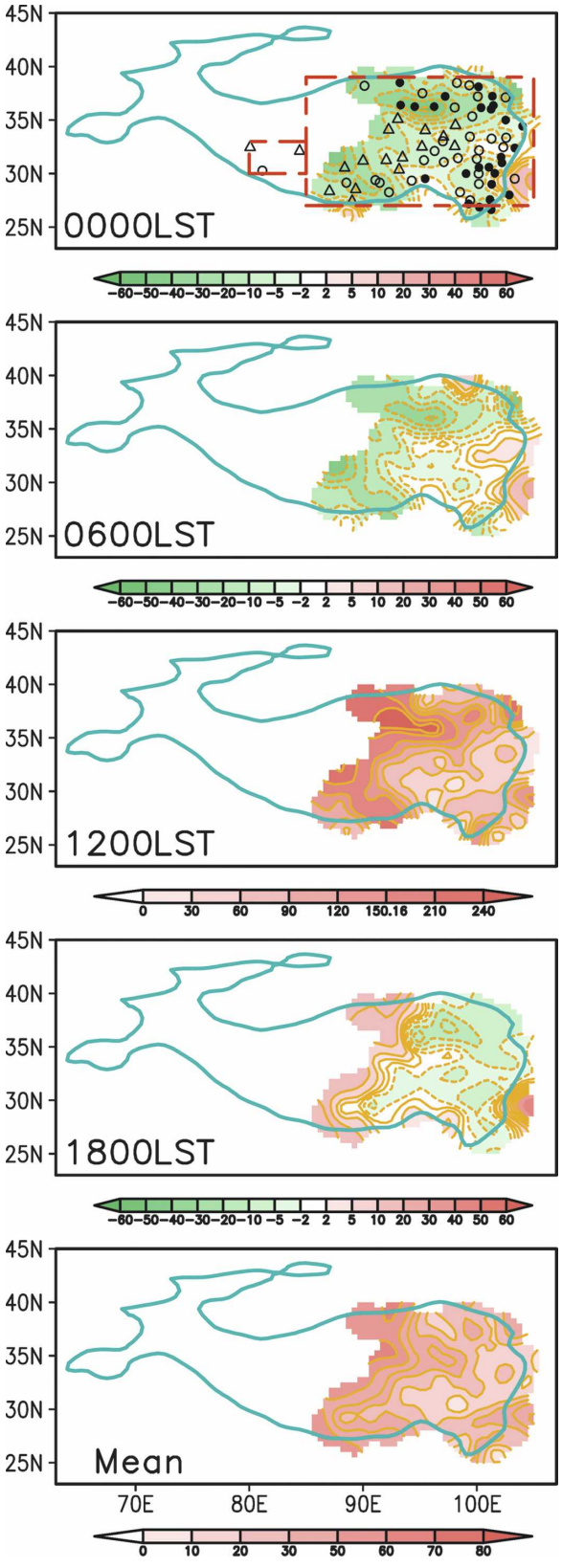


precipitation, and RC is the net radiation flux of the air column. We can calculate $E$ term by term or estimate it by using the apparent heat source $Q_1$ derived from the thermodynamic budget equation (Yanai 1961).

In this study, we calculate SH by the bulk aerodynamic method:

$$\mathrm{SH} = C_p \rho C_{\mathrm{DH}} V_0 (T_s - T_a), \tag{2}$$

where $C_p = 1005$ J kg$^{-1}$ K$^{-1}$ is the specific heat of dry air at constant pressure, $\rho$ is the air density that decreases exponentially with increasing elevation, $C_{\mathrm{DH}}$ is the drag coefficient for heat, and $V_0$ is the mean wind speed measured at 10 m above ground. This procedure is widely used in the TP-related studies (e.g., Yeh and Gao 1979; Chen et al. 1985; Li et al. 2001). The bulk aerodynamic method obviously depends on the choice of $C_{\mathrm{DH}}$, which varies from location to location (turbulence regime, surface roughness, and so on) and differs widely among different studies (Yeh and Wu 1998). For a fixed location and during our studied period from 1961 to 2003, the changes in $\rho$ and $C_{\mathrm{DH}}$ should be small, and their impacts on the change of SH are negligible. Therefore, the wind speed $V_0$ and ground–air temperature difference $(T_s - T_a)$ are the two key factors influencing the trend in SH. Here we assume $\rho = 0.8$ kg m$^{-3}$ (Yeh and Gao 1979) and $C_{\mathrm{DH}} = 4 \times 10^{-3}$ (Li and Yanai 1996) for the CE-TP and $C_{\mathrm{DH}} = 4.75 \times 10^{-3}$ for the W-TP (Li et al. 2000). These simplifications will not affect our final results.

Cautions are needed concerning the applicability of the bulk aerodynamic Eq. (2) to the TP studies. On the sloping lateral surfaces of the TP, because of the pumping effects of the TP SH driving air pump (TP-SHAP; Wu et al. 1997, 2007), ascending air flows penetrate the isentropic surfaces in sharp angles and compensate the surface SH. In such circumstances the heat flux is carried by thermal convection, and the time-mean surface SH can be formulated approximately as $(\mathbf{V}_0 \cdot \nabla\theta)$, where $\theta$ is potential temperature. However, over the vast TP platform, the near-ground $\theta$ surfaces become relatively flat, and the near-surface thermal advection becomes smaller as well. By employing four automatic weather stations over the TP, and using the gradient method, Li et al. (2000) calculated the SH based on (2)

←

FIG. 1. Annual-mean SH flux over the CE-TP during 1980–2003 in units of W m$^{-2}$. Note that contour intervals are different for each panel. (top) Triangles, open circles, and solid circles denote stations at or higher than 4000, 3000, and 2000 m, respectively. The thick curve outlines the TP area with an averaged altitude higher than 2500 m. Two dashed boxes in the top panel denote the (left) W-TP and (right) CE-TP areas.

and found that the results are comparable with other data outputs. In 1998, China launched the second TP field observation campaign with several observation sites located on the platform. By employing the corresponding observation data and comparing the results produced from different methods, Zhou et al. (2000) also indicated that the SH calculated based on (2) is comparable with those from other methods. These suggest that the bulk aerodynamic method be applicable over the TP platform. Nevertheless, to ensure that our analysis is reliable, the associated changes in wind speed $V_0$ and the land–air temperature difference ($T_s - T_a$) are also considered when investigating the change of SH.

LH can be calculated by precipitation via the following formula:

$$\mathrm{LH} = \mathrm{Pr} \times Lw \times \rho, \tag{3}$$

where $L_w = 2.5 \times 10^{-6}$ J kg$^{-1}$ is the condensation heat coefficient.

$$\begin{aligned} \mathrm{RC} &= R_\infty - R_0 \\ &= (S_\infty^\downarrow - S_\infty^\uparrow) - (S_0^\downarrow - S_0^\uparrow) - (F_0^\downarrow - F_0^\uparrow) - F_\infty, \end{aligned} \tag{4}$$

where $R_\infty$ and $R_0$ are the net radiation values at the top of the atmosphere and at the earth's surface, respectively. *V*ariables $S$ and $F$ denote shortwave and longwave radiation fluxes, the subscripts $\infty$ and 0 denote the top of the atmosphere and the ground surface, and the superscripts $\downarrow$ and $\uparrow$ represent downward and upward transports.

Simple linear regression is used to calculate the trend, and the sliding $t$ test is adopted to check the abrupt change. Using $x_i$ to indicate a climatic variable with a sample size $n$, and using $t_i$ to indicate the time corresponding to $x_i$, a linear equation is assumed to show the relationship between $x_i$ and $t_i$:

$$x_i = a + bt_i (i = 1, 2, 3, \ldots, n),$$

where $a$ and $b$ are the regression constant and linear regression coefficient [i.e., linear variation rate (LVR)], respectively. They can be estimated by using the least squares method:

$$b = \frac{\sum_{i=1}^{n} x_i t_i - \frac{1}{n}\left(\sum_{i=1}^{n} x_i\right)\left(\sum_{i=1}^{n} t_i\right)}{\sum_{i=1}^{n} t_i^2 - \frac{1}{n}\left(\sum_{i=1}^{n} t_i\right)^2},$$

$$a = \bar{x} - b\bar{t}, \quad \text{where} \tag{5}$$

$$\bar{x} = \frac{1}{n}\sum_{i=1}^{n} x_i, \quad \bar{t} = \frac{1}{n}\sum_{i=1}^{n} t_i.$$

After calculating $b$, a statistical test is employed to detect the significance of the trend. Here the correlation coefficient $r$ between $t$ and $x$ is examined: $|r| > 0.29$ and $|r| > 0.37$ denote that the LVR passes 95% and 99% confidence test for a 43-yr (1961–2003) sample size, and $|r| > 0.38$ and $|r| > 0.49$ denote the same for a 24-yr (1980–2003) sample size.

To compare the change in amplitudes of different variables with different units, the relative change rate (RCR) is also employed in this work, which is defined as,

$$\mathrm{RCR} = (B_e - B_b)/B_b, \tag{6}$$

where $B_e$ and $B_b$ are respectively the last/end and first/beginning values of the LVR of a time series. Unless stated otherwise, all significant changes reported in this study pass 95% confidence level.

## 3. Climatology of the atmospheric heat source/sink over the TP

Before discussing the trend of the heating status over TP, it is necessary to examine the climatology, in terms of spatial distribution and seasonal evolution.

### *a. CE-TP*

Figure 1 exhibits the annual-mean SH over the CE-TP during 1980–2003 at 0000, 0600, 1200, 1800 LST, and their daily mean. In general, 0000 and 0600 LST represent the night because it is still dark at 0600 LST most time of the year except for the midsummer. Most stations have negative SH at night, which results from a negative value of ($T_s - T_a$), thanks to warmer $T_a$ than $T_s$, and indicates the downward SH transfers from air to land surface. The minimum SH at 0000 LST exceeds $-60$ W m$^{-2}$ within Caidam basin (near 36°–37°N, 90°–97°E) which is located in the northern CE-TP. At noon (1200 LST), intensely positive SH spreads over the whole CE-TP region, with a maximum of above 240 W m$^{-2}$, again in Caidam basin. The intensity in the central and northern TP is notably larger than that in the southeast TP. The noticeable difference in SH across the TP is directly related to the complex orography, underlying surface characteristics, and local climate. As is well known, the eastern TP is characterized by relatively lower elevation, abundant vegetation, and a warm and humid climate, while the W-TP is characterized by higher elevation, sparse vegetation, and a semiarid climate. Hence the magnitude of SH over the CE-TP is reasonably smaller than that over the W-TP, as will be shown later. The average SH at local midday for the CE-TP region is around 100 W m$^{-2}$, approximately equivalent to 10 K day$^{-1}$ heating rate in the surface air

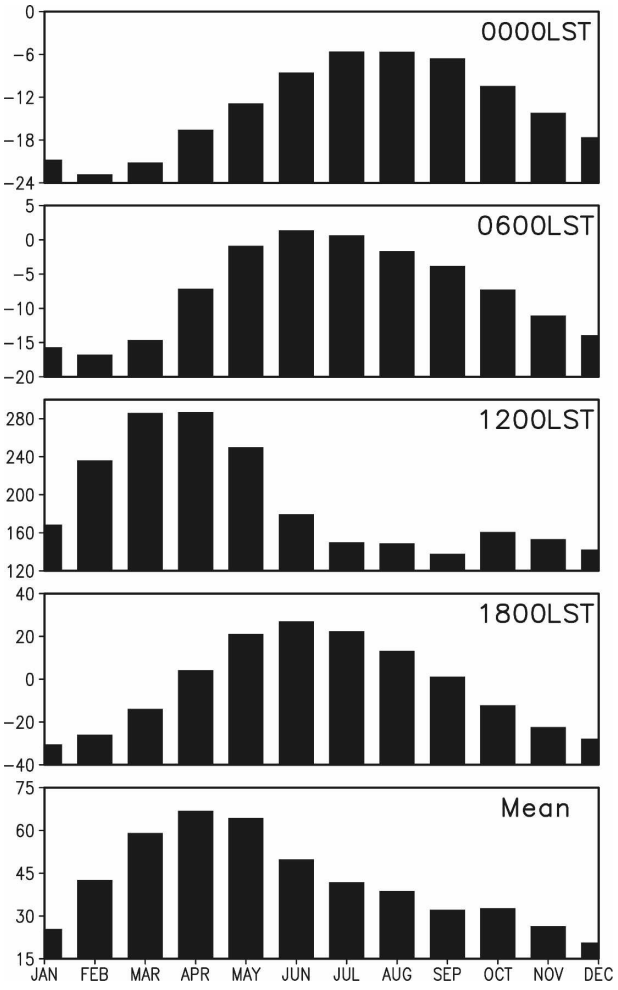


FIG. 2. Annual cycle of the 71-station-averaged SH over the CE-TP during 1980–2003 in units of W $m^{-2}$.

layer. This is the reason why the TP is called a gigantic SH air pump (Wu et al. 1997, 2007), which generates the deep and well-mixed layer of potential temperature and tropospheric heating in the afternoon (Luo and Yanai 1983; Yanai and Li 1994). At 1800 LST, which is before sunset in the central TP but after sunset in the eastern TP for most parts of the year, SH remains positive to the west of 90°E but becomes negative to the east. For the annual mean, the 71-station-averaged SH over the CE-TP is ~40 $Wm^{-2}$, which is about half of that given by Yeh and Gao (1979), who set the $C_{DH}$ as high as $8 \times 10^{-3}$, but it agrees well with Chen et al. (1985) and Zhao (1999). It is worth noting that the strongest SH source or sink is located in the northern TP instead of the central TP.

The annual cycle of SH averaged over the 71 stations and for the period 1980–2003 is displayed in Fig. 2. The SH at midnight (0000 LST) is always negative throughout the year. It increases from the minimum of −22.8 W $m^{-2}$ in February to the maximum of −5.8 W $m^{-2}$ in July, and then gradually decreases to the minimum. The SH at dawn (0600 LST) is transferred from air to land surface year round except for June and July, reaching the minimum in February and the maximum (1.4 W $m^{-2}$) in June. The perennial strong surface SH at local midday (1200 LST) ranges from 138 W $m^{-2}$ (in September) to 287 W $m^{-2}$ (in April), and exceeds 200 W $m^{-2}$ from February to May. The SH at 1800 LST is positive from April to September and negative during the rest months, with the maximum of 23 W $m^{-2}$ in June and the minimum of −30 W $m^{-2}$ in January. Since the SH at noon is one order larger, the daily-mean SH exhibits a similar change with its maximum of 67 W $m^{-2}$ in April and minimum of 21 W $m^{-2}$ in December.

Because of the lack of 6-hourly precipitation data, the climatology of the seasonally averaged LH over the CE-TP is calculated instead (Fig. 3). Large LH occurs over the southeast and south-central parts of the plateau, with maximum values along the valley of the Yarlung Zangbo Jiang (Brahmaputra River). LH decreases gradually toward northwest. One prominent feature of the TP climate is the vigorous summer monsoon, and the magnitude of LH in JJA is much larger than other times of the year. During the rainy season, LH over most areas usually exceeds 80 W $m^{-2}$ (about 3 mm $day^{-1}$ rainfall), overwhelming SH or RC over the TP.

Domain-averaged ISCCP data are used to estimate the net RC over the TP. The data at the 54 grids in the CE-TP and at the 6 grids in the W-TP are extracted and averaged to obtain RC for each region. The RC averaged from the 54 grids together with the 71-station-averaged SH and LH is shown in Table 1 to show the magnitudes of the individual components of $E$ in the CE-TP. Clearly, the TP is an atmospheric heat source in spring [March–May (MAM)] and summer [June–August (JJA)], but becomes a heat sink in autumn [September–November (SON)] and winter [December–February (DJF)]. Most contributions to the total diabatic heating come from SH in MAM and from LH in JJA, which is usually more than twice the SH in summer. On the other hand, RC ranges from −60 to −90 W $m^{-2}$, always tending to make the air column a heat sink. Despite many differences in details, the results demonstrated here agree qualitatively with those given by Yeh and Gao (1979), Chen et al. (1985), Zhao and Chen (2001), and DW05.

### *b. W-TP*

Both the diurnal and annual ranges of SH in the W-TP are noticeably larger than those in the CE-TP.

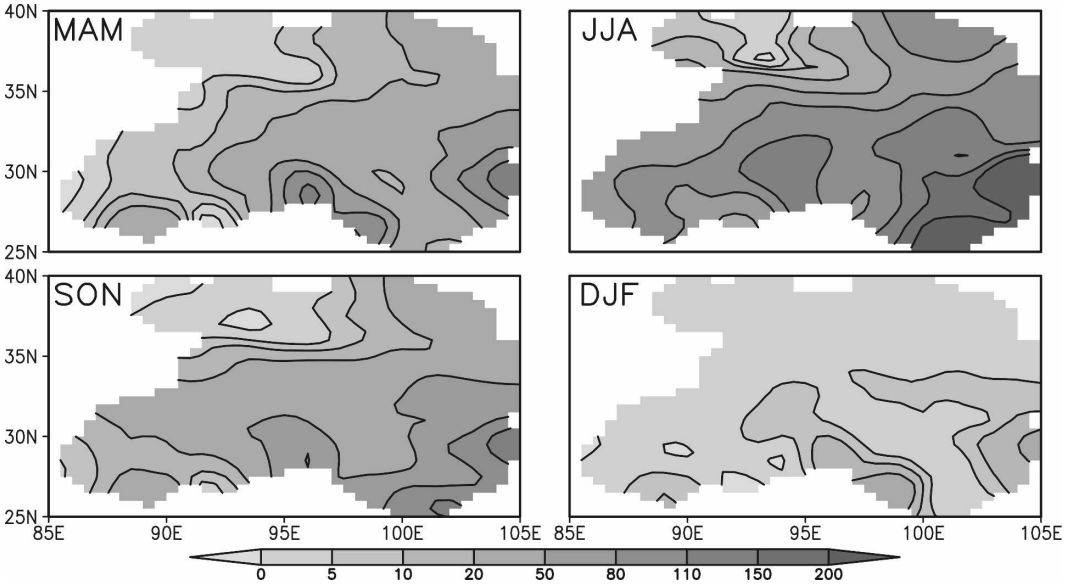


FIG. 3. Seasonal-mean LH flux over the CE-TP during 1980–2003 in units of W $m^{-2}$.

Figure 4 and Tables 1 and 2 exhibit the climatology of SH in W-TP (calculated with aforementioned three stations). The strongest SH with the intensity of 290 W $m^{-2}$ at 1200 LST and the largest diurnal range with the value of 332.8 W $m^{-2}$ are detected at Gaize, but the daily-mean SH at this station (63.7 W $m^{-2}$) is smaller than that at Shiquanhe (76.2 W $m^{-2}$). The diurnal range of SH in the W-TP even exceeds 400 W $m^{-2}$ in May, and the annual range of daily-mean SH is more than 100 W $m^{-2}$. Furthermore, the SH maximum in the W-TP lags that in the CE-TP by one or two months except for 1800 LST. This phenomenon is directly related to the fact that the rainy season starts first in the southeastern TP from late April to early May and then propagates westward until it reaches the W-TP in late June or early July (Yeh and Gao 1979).

As shown in Table 1, the seasonal evolution of E in the W-TP is very different from that in the CE-TP. The LH in the W-TP is always a small term in the energy budget (1). The spring heat source over the W-TP is two times larger than that over the CE-TP. The SH in MAM and JJA exceeds 100 W $m^{-2}$, about double that in the CE-TP. Nevertheless, the atmospheric heat sink in SON and DJF is weaker than that in the CE-TP mainly because of the lower RC.

In general, the TP acts as an especially strong sensible heat source in spring and summer with the daily maximum in the local afternoon. A distinct feature of the SH over the TP is the large diurnal range but much weaker annual range. Both the diurnal and annual ranges decease gradually from northwest toward southeast, while the annual cycle over the semiarid W-TP lags that over the humid CE-TP by about one month.

TABLE 1. Climatology (1984–2003) of the atmospheric heat source/sink and each component over TP in units of W $m^{-2}$.

| Region | Component | MAM | JJA | SON | DJF | Annual |
|---|---|---|---|---|---|---|
| CE-TP | SH | 62 | 42 | 29 | 27 | 40 |
| | LH | 30 | 101 | 37 | 4 | 43 |
| | RC | −61 | −80 | −90 | −81 | −78 |
| | *E* | 31 | 63 | −24 | −50 | 5 |
| W-TP | SH | 102 | 101 | 47 | 15 | 66 |
| | LH | 6 | 25 | 6 | 4 | 10 |
| | RC | −45 | −63 | −64 | −63 | −59 |
| | *E* | 63 | 63 | −11 | −44 | 18 |

## 4. Trend in SH over the TP

### *a. Trends in SH at different times of the day*

Because SH reaches its daily minimum and maximum at the night and the afternoon, respectively, in Fig. 5 we show the time sequences of $T_a$, $T_s$, $V_0$, and SH at 0000 and 1200 LST for the CE-TP to estimate their long-term trends and to find out their differences between day and night.

At 0000 LST, $T_a$ increases rapidly after the late 1960s and reaches the peak at 1999. The LVR during 1961–2003 is of 0.29°C $decade^{-1}$ and the trend is above 99.9% confidence level. The most significant (above 99.9% confidence level) abrupt warming is detected in 1986. The increase in $T_a$ is more evident during 1980–2003, and its LVR is 0.4°C $decade^{-1}$ for the 71-station

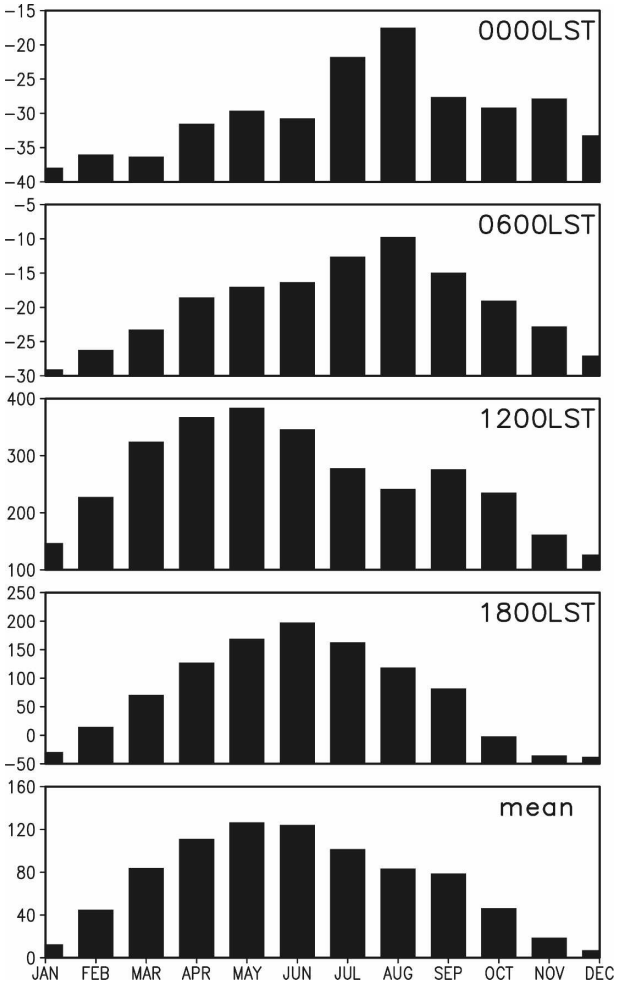


FIG. 4. Annual cycle of the three-station-averaged SH over the W-TP during 1980–2003 in units of W $m^{-2}$.

average. Note that both the interannual variation and long-term trend of the 71-station-averaged $T_a$ are very similar to those of 37-station-averaged $T_a$ during 1980–2003. This gives us confidence in using the 37 stations for the CE-TP during the whole period 1961–2003.

At 0000 LST, $T_s$ and $T_a$ have similar interannual variations and decadal trend. The LVR of $T_s$ during 1961–2003 is 0.2°C $decade^{-1}$, and the LVR for 71-station-averaged $T_s$ during 1980–2003 is 0.37°C $decade^{-1}$. Both the trend in $T_s$ and its abrupt warming in 1986 are statistically significant. Smaller increase in $T_s$ than in $T_a$ leads to a reduction in $(T_s - T_a)$. On the other hand, $V_0$ decreases continuously since the early 1970s with a LVR of −0.09 $(ms^{-1})$ $decade^{-1}$. The decrease in $V_0$, together with the reduction in $(T_s - T_a)$ due to the larger increase in $T_a$ than in $T_s$, leads to a persistent increase of nocturnal SH since 1973. This implies decreased SH transfer from air to land surface. The LVR of SH at 0000 LST during 1961–2003 is 0.3 (W $m^{-2}$) $decade^{-1}$, and the LVR during 1980–2003 for the 71-station average is 1.2 (W $m^{-2}$) $decade^{-1}$. The increasing trend at 0000 LST is significant only during 1980–2003.

TABLE 2. Annual-mean SH and its diurnal range at three stations in the W-TP during 1980–2003 in units of W $m^{-2}$.

| Station | 0000 LST | 0600 LST | 1200 LST | 1800 LST | Daily mean | Diurnal range |
|---|---|---|---|---|---|---|
| Shiquanhe | −25.9 | −13.5 | 255.7 | 88.4 | 76.2 | 281.6 |
| Caze | −42.8 | −24.7 | 290.0 | 28.6 | 63.7 | 332.8 |
| Pulan | −21.0 | −21.0 | 234.1 | 94.0 | 71.5 | 255.1 |

The trends in $T_a$ and $V_0$ at 1200 LST are similar to those at 0000 LST, except for small changes in amplitude. During 1961–2003, the LVRs of $T_a$ and $V_0$ are 0.2°C·$decade^{-1}$ and −0.06 $(m\,s^{-1})$ $decade^{-1}$, respectively. However, the trends in $T_s$ during 1961–2003 for the 37-station average and that during 1980–2003 for the 71-station average are opposite, with the LVRs of −0.19°C $decade^{-1}$ and 0.47°C $decade^{-1}$, respectively. The combined effect of the changes in $T_a$ and $T_s$ lead to a decreasing trend of $(T_s - T_{a)}$ during 1961–2003 but a slightly increasing trend during 1980–2003 (figures not shown here). Similar to 0000 LST, the surface wind speed $V_0$ at 1200 LST decreases significantly since 1970s. The weakened $V_0$ induces a significant weakening trend of SH at noon with the LVR of −16.3 $(Wm^{-2})$ $decade^{-1}$ during 1980–2003.

Because the daily maximum SH usually occurs at noon, and because the SH trend at 1200 LST declines remarkably, a significant decreasing trend of the daily-mean SH then occurs during 1980–2003 over the CE-TP. During this period, an increasing trend of 0.68 (W $m^{-2}$) $decade^{-1}$ exists at 0600 LST, while a decreasing trend of −0.03 (W $m^{-2}$) $decade^{-1}$ exists at 1800 LST. Therefore, the long-term trend in SH over the CE-TP can be summarized as a weaker increasing trend at night and a stronger decreasing trend during day.

### b. Trends in SH during winter and spring

As shown in section 3, the annual minimum and maximum SH over the CE-TP occur in DJF and MAM, respectively. Figure 6 shows the long-term trends in SH during these two seasons. Both $T_a$ and $T_s$ increase significantly during 1980–2003 regardless of seasons. However, the increase in DJF is more rapid in $T_a$ (0.49°C $decade^{-1}$) than in $T_s$ (0.42°C $decade^{-1}$), which lead to a slightly decreasing trend of $(T_s - T_a)$ of −0.07°C $decade^{-1}$. The opposite happened in MAM, the increase in $T_s$ (0.4 $decade^{-1}$) is more rapid than that in

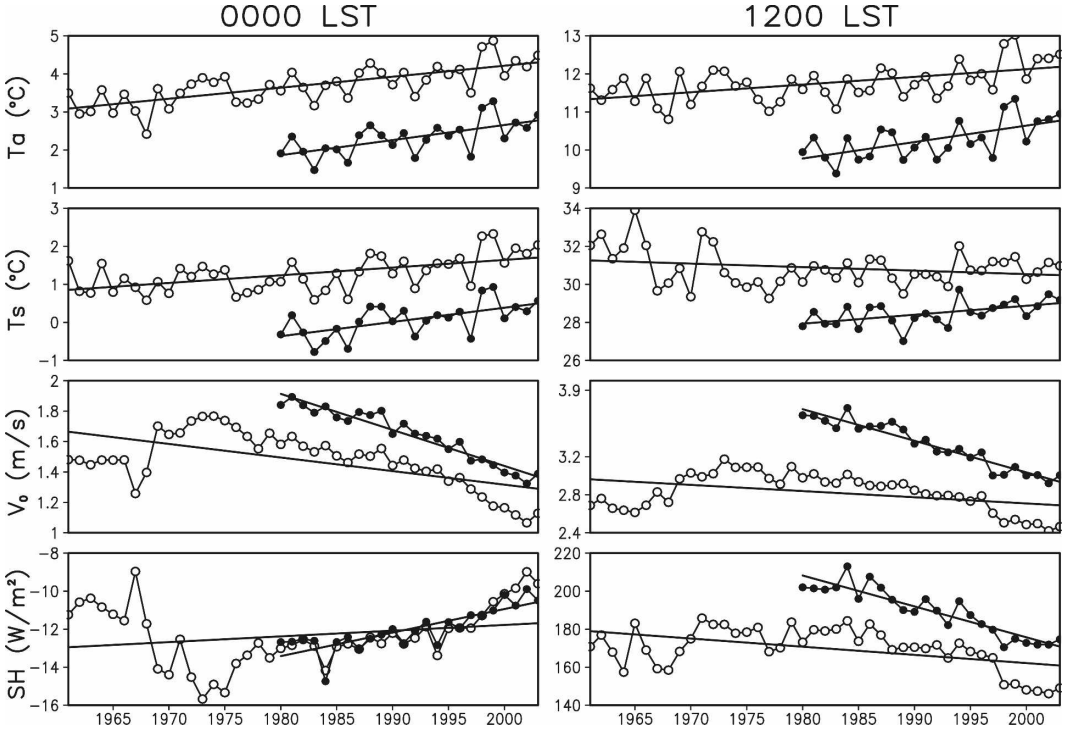


FIG. 5. Temporal evolution of (top) $T_a$, (upper middle) $T_s$, (lower middle) $V_0$, and (bottom) SH over the CE-TP at (left) 0000 and (right) 1200 LST. The units of $T_a$ and $T_s$ are °C, $V_0$, m s$^{-1}$, and SH, W m$^{-2}$. Curves with open circles are 71-station averaged, and curves with closed circles are 37-station averaged.

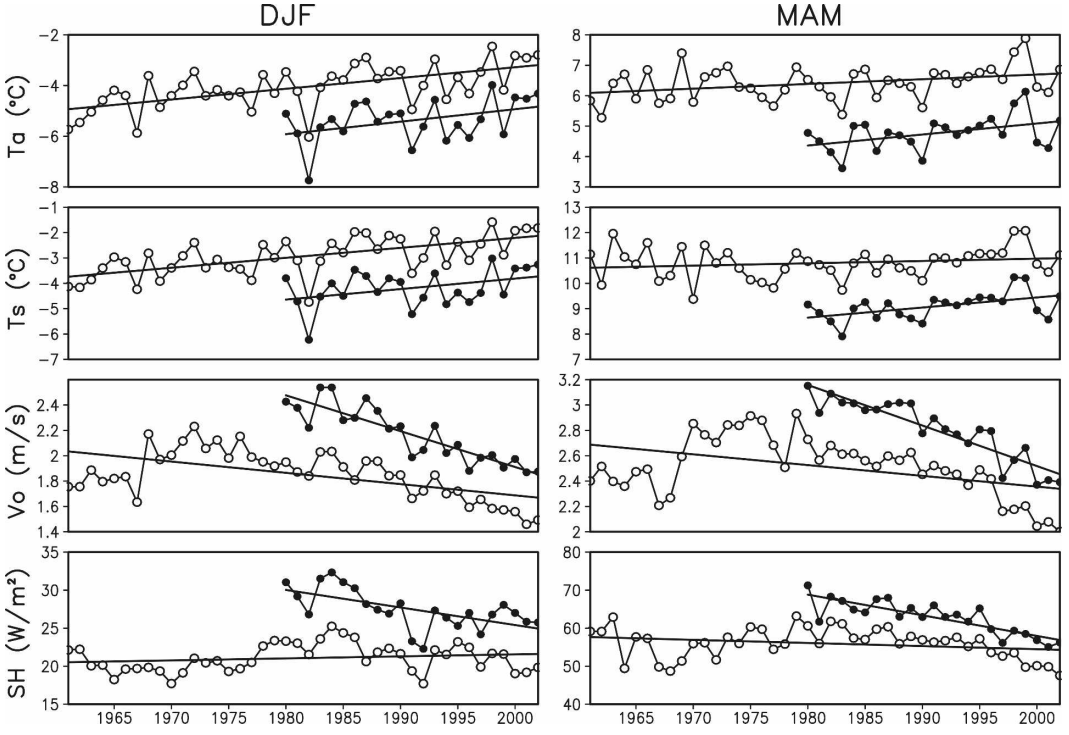


FIG. 6. Same as Fig. 5, except for (left) DJF and (right) MAM.

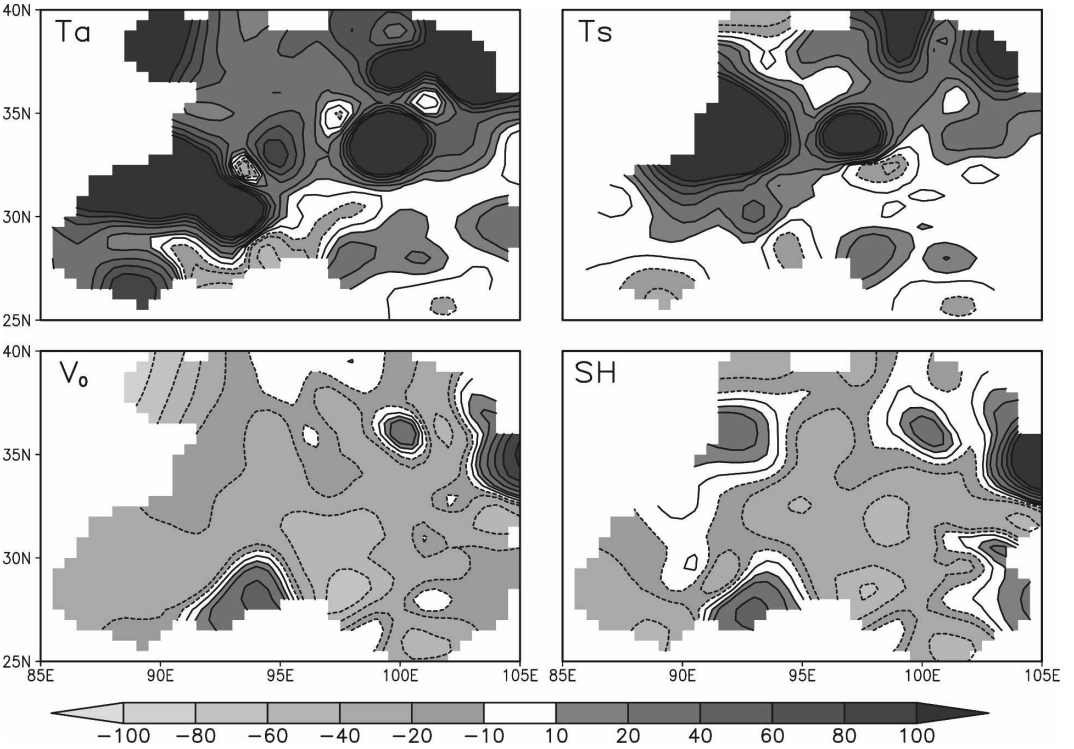


FIG. 7. Spatial distribution of RCR in units of % over the CE-TP during 1980–2003.

$T_a$ (0.36°C decade$^{-1}$), which lead to a slightly increasing trend of ($T_s - T_a$) of 0.04°C decade$^{-1}$. On the other hand, $V_0$ decreases sharply since 1970s. This causes a decreasing trend in DJF ($-2.3$ (W m$^{-2}$) decade$^{-1}$) and a larger decreasing trend in MAM ($-5.4$ (W m$^{-2}$) decade$^{-1}$). As a result, a diminished annual cycle of SH over the CE-TP is observed. For summer and autumn, decreasing SH trends are also significant with the LVRs of $-3.1$ and $-2.6$ (W m$^{-2}$) decade$^{-1}$, respectively (figures not shown).

### c. Spatial distribution of the SH trend

Because of the vast domain with complicated topography, climate change over the TP may vary with locations. To compare the change in terms of amplitude among various meteorological variables over the CE-TP, Fig. 7 shows the spatial distribution of RCR given by Eq. (6) for $T_a$, $T_s$, $V_0$, and SH over the CE-TP during 1981–2003. In contrast to the almost coherent increases in $T_a$ and $T_s$ across the CE-TP, $V_0$ and SH experience obvious decreasing trend for most parts of the CE-TP. The 71-station-averaged RCR of $T_a$, $T_s$, $V_0$, and SH are 57%, 32%, $-22$%, and $-14$%, respectively. Only 11 of the 71 stations show an increasing trend in SH. It is necessary to note that the change in $T_a$, $T_s$, $V_0$, and SH is not linearly correlated with elevation.

Over the W-TP (Fig. 8), positive trends of $T_a$, $T_s$, and negative trend of $V_0$ at both 0000 and 1200 LST are as the same as their counterparts over the CE-TP. Because of varying $V_0$ and ($T_s - T_a$) at the three stations, the LVRs of SH are also be different throughout the whole period. An abrupt change point in SH at 1200 LST can be detected. The SH shows an increasing trend before 1989 and a decreasing trend afterward. Therefore, there is a decreasing trend in SH over the W-TP, with the largest amplitude in spring (Table 3).

### d. Relationship with the declined East Asian summer monsoon

As the primary heat source before the rainy season (e.g., Yeh and Gao 1979; Yanai et al. 1992), SH over the TP exerts a significant influence on the East Asian summer monsoon in terms of both the timing of the onset (Wu and Zhang 1998) and the subsequent rainfall pattern and intensity (Zhao and Chen 2001; Duan et al. 2005). The above-normal SH over the TP before July may lead to positive rainfall anomalies over the TP, along the reaches of the Yangtze and Huaihe Rivers, in the Sichuan basin, and over the Yunnan-Guizhou Plateau, but negative rainfall anomalies in the regions over the north, northeast, and west of the TP. On decadal time scales, the significant weakening trend of the

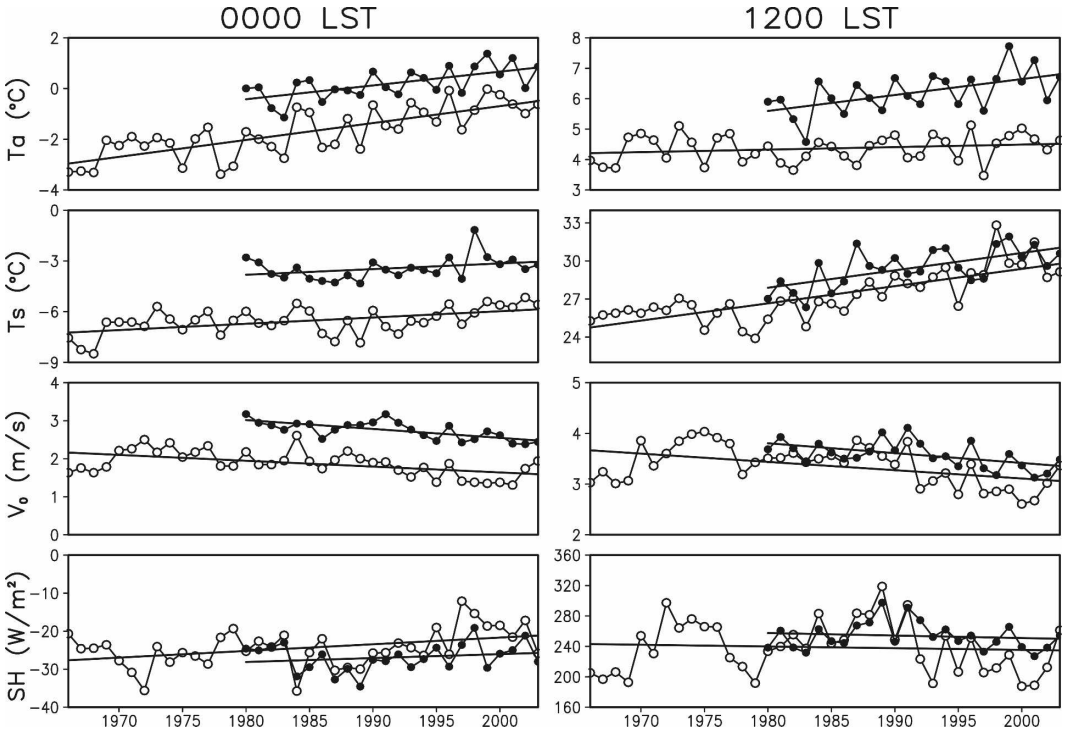


FIG. 8. Same as Fig. 5, except for the W-TP. Curves with open circles are for Shiquanhe, and curves with closed circles denote the average of the three stations, namely, Shiquanhe, Gaze, and Pulan.

spring SH over the TP may modulate the East Asian summer monsoon to some degree.

As a matter of fact, the surface wind speed over most parts of China shows a steady declining trend during 1969–2000, accompanied by the decreased winter and summer monsoons in East Asia (Xu et al. 2006). This results in increased droughts in the northern China and flood along the Yangtze River Valley (Yu et al. 2004). Xu et al. (2006) argued that the decline of the summer monsoon is linked to the summer cooling in central South China, which is likely induced by the air pollution, as well as by the warming over the South China Sea and the western North Pacific Ocean. However, the mechanism for the decadal trend in the East Asian summer monsoon may be more complicated. As shown earlier, the steady decline of $V_0$ over the TP starts in early 1970s as well, implying that a similar mechanism may exist. And this mechanism is more likely related to the global circulation shift. The connection between the trends in SH over the TP and the global circulation shift will be discussed in section 6. It is not yet clear how the suppressed summer monsoon is linked to the SH trends over the TP, a puzzle that needs future investigation.

TABLE 3. Trend in the atmospheric heat source/sink $E$ and its components over the TP in units of (W m$^{-2}$) decade$^{-1}$. Analysis period for SH and LH is 1980–2003 and for RC is 1984–2004.

| Region | Component | MAM | JJA | SON | DJF | Annual |
|---|---|---|---|---|---|---|
| CE-TP | SH | −5.4 | −3.1 | −2.6 | −2.3 | −3.4 |
| | LH | 1.5 | 0.5 | 0.4 | 0.3 | 0.7 |
| | RC | −8.1 | −9.7 | −14.4 | −12.7 | −11.2 |
| | $E$ | −12.0 | −12.3 | −16.6 | −14.7 | −13.9 |
| W-TP | SH | −3.0 | −6.1 | 0.2 | 1.1 | −2.0 |
| | LH | −1.4 | 1.3 | −1.6 | 0.4 | 0.3 |
| | RC | 4.5 | −3.6 | −7.0 | −1.4 | −1.8 |
| | $E$ | 0.1 | −8.4 | −8.4 | 0.1 | −4.2 |

## 5. Trend in LH and RC over the TP

The trends in LH and RC over the TP are further investigated here. In contrast to the weakening trend of the surface heat source, an evident strengthening trend of LH over the CE-TP exists in MAM and DJF (Fig. 9). Spatial distribution of the trend of LH varies with seasons. A widespread increasing trend can be detected in MAM except at few stations located in the northeast and southeast TP. However, the JJA is featured by a pattern with an increasing trend in the north and south TP but a decreasing trend in the middle. The pattern in SON is somewhat similar to that in MAM but with a larger area of weakening trend in the eastern plateau. Precipitation in DJF is much less than the rest of the

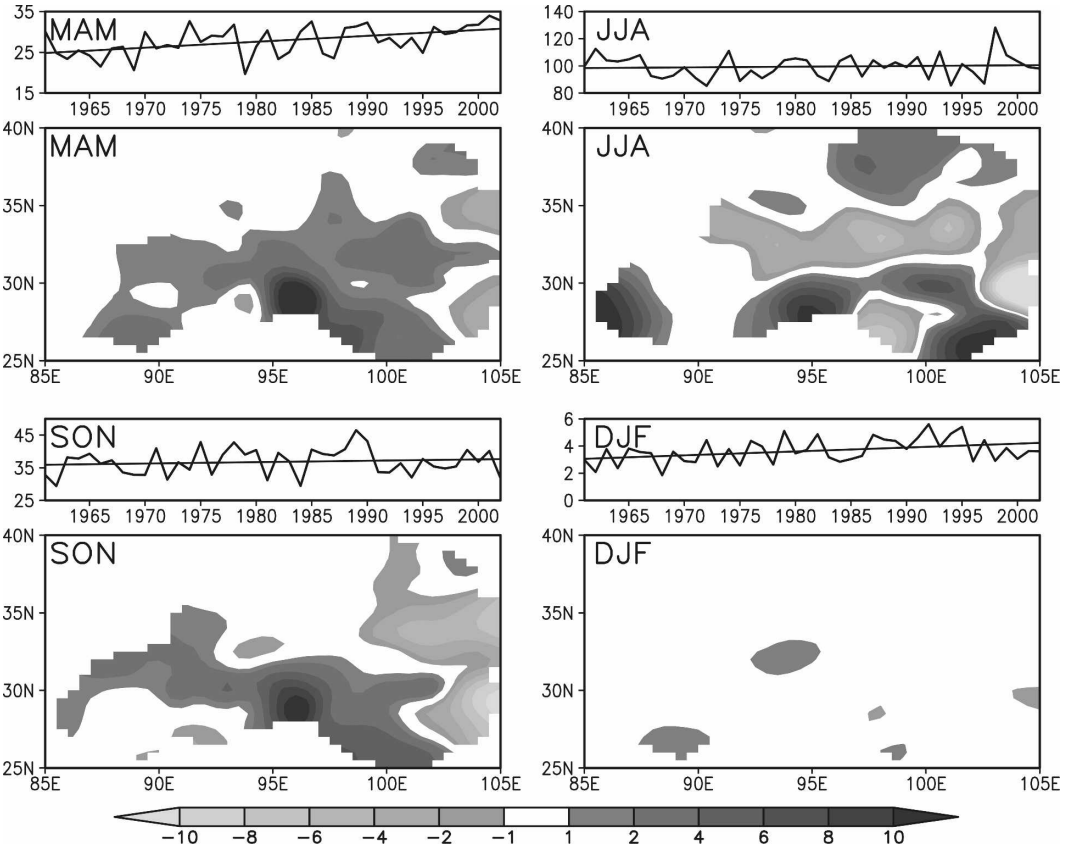


FIG. 9. Temporal evolution (W $m^{-2}$) and spatial distribution [(W $m^{-2}$) $decade^{-1}$] of the LVR of LH in four seasons over the CE-TP during 1961–2003.

year, but it does exhibit a significant growing trend, especially in the middle of the CE-TP. This induces a positive trend in LH. These results are consistent with earlier studies that showed snow depth over the TP increases persistently during the recent decades (Zhang et al. 2004).

Figure 10 shows the temporal evolution of the domain-averaged net shortwave and longwave radiation fluxes, and their combination term (RC) over the CE-TP and W-TP during 1984–2004. The heating effect from solar radiation and cooling effect from longwave radiation are enhanced simultaneously over the whole TP area. However, the decrease in longwave radiative cooling is stronger, which leads to an intensified RC, especially over the CE-TP. The change of radiation effect in atmosphere is closely related to the change of the in situ cloud. Based on the observations from the same stations as used in this study, DW06 showed that the total cloud amount over the TP area decreases persistently since the mid-1970s. Therefore the increase trends in shortwave heating as well as in longwave cooling as shown in Fig. 10 may be related to the reduced cloud amount over the TP. However, the physical and chemical processes responsible for the change of cloud amount are complicated and beyond the scope of this study.

The trends of $E$ and its individual components are

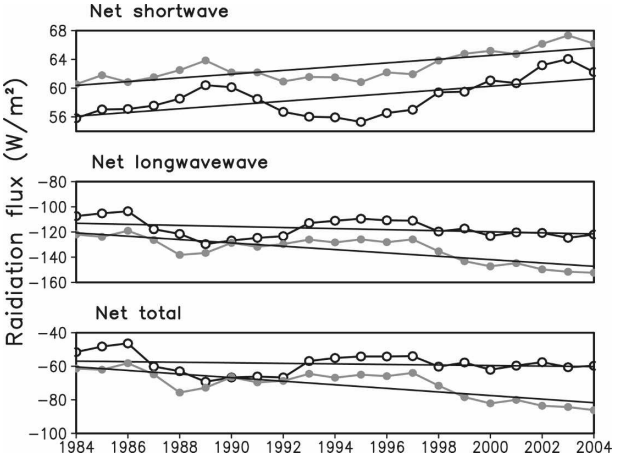


FIG. 10. Temporal evolutions of the annual-mean radiation flux in units of W $m^{-2}$ of the air column over the CE-TP (solid circle) and the W-TP (open circle) in 1984–2004.

summarized in Table 3. Because of the difference in data length between the station observations and ISCCP satellite observations and the difference between using station average and domain average, some inconsistency may occur when using these datasets. But the resulted errors should be small because of the huge sample size of the data. Over the CE-TP, both SH and RC exhibit a decreasing trend in all seasons, though the amplitude of the latter is clearly larger than the former. Although the LH presents a reversed increasing trend throughout the whole year, it is too small to compensate the weakening effect induced by the decreasing trend in either SH or RC. The trend in annual-mean SH and LH during 1980–2003 are $-3.4$ and 0.7 (W m$^{-2}$) decade$^{-1}$, respectively, and the trend in annual-mean RC during 1984–2004 is $-11.2$ (W m$^{-2}$) decade$^{-1}$. Therefore, the annual-mean atmospheric heat source decreases at a rate of about $-13.9$ (W m$^{-2}$) decade$^{-1}$ during the last two decades.

The air column integrated diabatic heating over the W-TP is also featured by a negative trend, though some differences between the W-TP and the CE-TP exist. For instance, the largest weakening for SH occurs in summer [$-6.1$ (W m$^{-2}$) decade$^{-1}$] instead of in spring [$-3.0$ (W m$^{-2}$) decade$^{-1}$], and small positive trends exist in autumn [0.2 (W m$^{-2}$) decade$^{-1}$] and winter [1.1 (W m$^{-2}$) decade$^{-1}$]. The trend in LH is characterized by a weakening in spring [$-1.4$ (W m$^{-2}$) decade$^{-1}$] and autumn [$-1.6$ (W m$^{-2}$) decade$^{-1}$], but a strengthening in summer [1.3 (W m$^{-2}$) decade$^{-1}$] and winter [0.4 (W m$^{-2}$) decade$^{-1}$]. Hence its annual change is negligible [0.3 (W m$^{-2}$) decade$^{-1}$]. RC intensifies for much of the year except in spring [4.5 (W m$^{-2}$) decade$^{-1}$], and it contributes to tamper the heat source over the W-TP with an annual trend of $-1.8$ (W m$^{-2}$) decade$^{-1}$. All these changes generate an annual trend for the entire air column of $-4.2$ (W m$^{-2}$) decade$^{-1}$, which is particularly significant in summer and autumn [$-8.4$ (W m$^{-2}$) decade$^{-1}$ in both].

In summary, because of the overwhelming role of the SH before the summer monsoon onset and the much larger decreasing trend in SH and RC than the increasing trend in LH, the atmosphere heat source over the TP losses its strength in all seasons. In addition, the weakening trend in SH is more evident over the CE-TP than over the W-TP, and more evident in spring and summer than in autumn and winter.

## 6. Relationship between changes in SH over the TP and the general circulation

We have shown that during the past two decades the surface wind speed and sensible heat flux over the TP have weakened. The question is whether the weakening SH over the TP is only a localized phenomenon or it is a result of the global climate change. We hope to address at least some aspects of this issue here.

Surface sensible heating is a shallow layer in the atmosphere. Its impact decreases upward exponentially and vanishes by $\sigma = 0.8$ ($\sigma$ = pressure/surface pressure). The atmospheric thermal adaptation to the surface sensible heating is characterized by generating cyclonic vorticity in a shallow layer near the surface and anticyclonic vorticity in a deep layer aloft (e.g., Wu and Liu 2000; Wu et al. 2004; Yanai and Wu 2006). Yanai and Li (1994) confirmed that, over the TP before the monsoon onset when SH contributes significantly to the total heating, there is a large ($T_s - T_a$) and strong SH during the day, which generates a thin layer of superadiabatic lapse rates near the surface, a low-level warm low at around ~600 hPa, and the strong dry convection over the TP. Accompanying the weakening SH, an increased surface pressure and thus a weakened warm low in the surface layers appears above the TP (figure not shown). This indicates that the diminished ($T_s - T_a$) and SH over the TP during the last two decades have contributed to the weakened the surface cyclonic circulation.

The stratosphere is one of the key players in determining the memory of the climate system (Baldwin et al. 2003). Figure 11 presents the LVRs of air temperature, geopotential height, and wind speed during 1980–2004, which are averaged from the 12 radiosonde stations in the TP. There exist a clear cooling trend in the upper troposphere and lower stratosphere (UTLS) and a warming trend in the mid- and lower troposphere (MLT) over the TP. Cooling in the UTLS exists in February, May, and August, as three centers of above $-1.2$°C decade$^{-1}$, while warming in the MLT is much weaker with two centers of about 0.3°C decade$^{-1}$ in March and May. Similar results can be seen in Fig. 2 of Zhou and Zhang (2005). They found that ozone depletion in the UTLS is particularly obvious in winter and spring over the TP, which induces less absorbing solar radiation in the UTLS but more in the MLT and caused cooler UTLS and warmer MLT.

As a result of the temperature change, the geopotential height displays a decreasing trend in the UTLS and an increasing trend in the MLT (Fig. 11b). Consistent with the seasonally dependent change of temperature, the largest geopotential height increase occurs in late winter and early spring with the average LVR of more than 1 dagpm decade$^{-1}$.

The change of wind speed seems more complicated (Fig. 11c). Although for the most part of the year (except for May and November) there exist a weakening

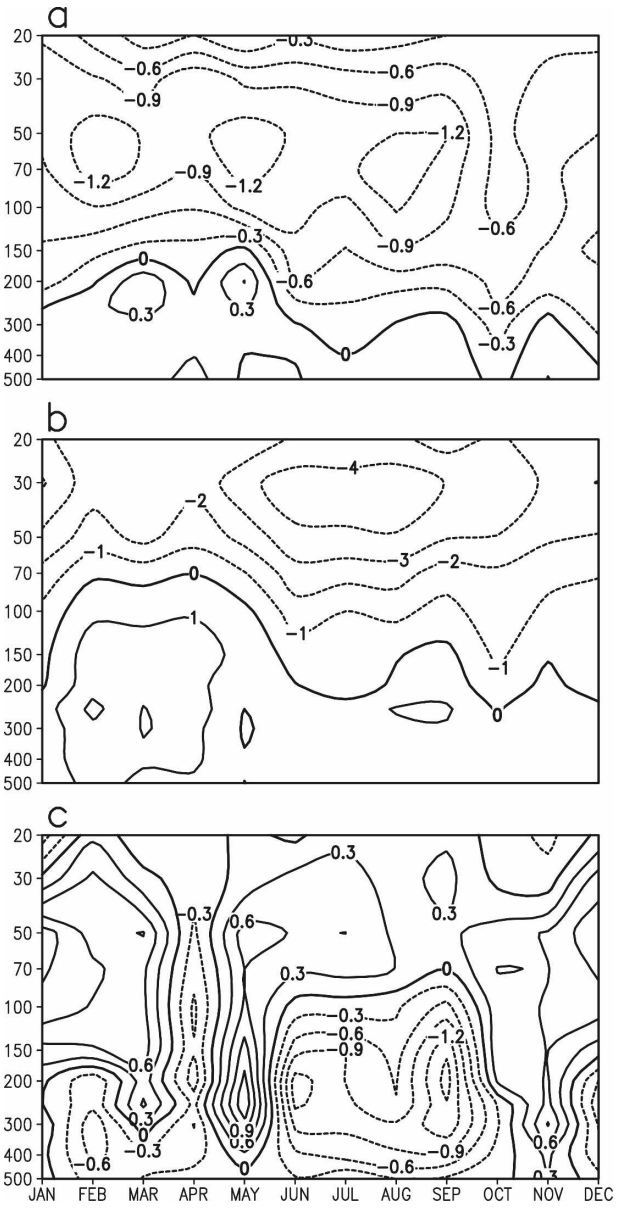


FIG. 11. Time–altitude sections of the linear trends for (a) air temperature (°C decade$^{-1}$), (b) geopotential height (dagpm decade$^{-1}$), and (c) wind speed [(m s$^{-1}$) decade$^{-1}$] as averaged from the 12 radiosonde stations over the TP during 1980–2003. Dashed lines are for negative trends.

trend in the troposphere and an intensifying trend in the stratosphere. The largest weakening trend [−1.2 (m s$^{-1}$) decade$^{-1}$] in tropospheric wind speed occurs during summer season (June to September) rather than in spring. However, a peculiar strengthening trend happens in May and November [0.3–1.2 (m s$^{-1}$) decade$^{-1}$]. These two months are normally transition seasons between winter and summer, when the subtropical westerly jet retreats northward or marches southward across the TP. The trend then indicates an increasing westerly over the TP during the transition seasons, which might influence the climate downstream.

The changes in temperature and geopotential height (Figs. 11a,b) show that the variations in the UTLS and the MLT have opposite signs. In spring, the altitudes of the positive trends in temperature and geopotential height even reach the tropopause. This certainly cannot be explained as a local response to the decreasing trend in SH over the TP, since the latter would generate a positive geopotential height trend and a negative temperature trend only near the surface according to the thermal adaptation theory. On the other hand, the weakening and strengthening trends in the wind speed over the TP occur throughout the whole troposphere. They are related to the changes in advection, Coriolis force, and pressure gradient terms in the momentum equation. We may infer that the weakening in surface wind speed and SH over the TP during the last two decades is associated with the global climate change. The confirmation of this inference, however, requires further investigation.

## 7. Summary and discussion

Using historical records, we have demonstrated that both SH and RC over the plateau underwent pronounced changes when a striking climate warming occurred there during the last two decades. The main findings are summarized as follows:

1) A statistically significant decreasing trend in SH during the last two decades has been detected in the CE-TP. The linear tendency of 71-station-averaged SH during 1980–2003 is −3.8 (W m$^{-2}$) decade$^{-1}$ with a relatively decreasing rate of −14%. The largest decreasing trend occurs at local noon and in spring when SH reaches the daily and annual maxima. It in turn leads to the reduction in both the diurnal and annual ranges of SH.
2) Meanwhile, a relatively weaker increasing trend in LH [0.7 (W m$^{-2}$) decade$^{-1}$] during 1980–2003 and a stronger decreasing trend in RC [−11.2 (W m$^{-2}$) decade$^{-1}$] during 1984—2003 are also detected. The combination of these changes leads to a weakened atmospheric heating in spring and summer and an enhanced cooling in autumn and winter over the CE-TP.
3) The annual-mean atmospheric heat source over the W-TP also declines [−4.2 (W m$^{-2}$) decade$^{-1}$] mainly because of the weakened SH in spring and summer and the enhanced RC in summer and autumn.

4) The decreasing trend in SH over the TP is induced mainly by the reduced surface wind speed, and also influenced to a certain degree by the diminished ground–air temperature difference. Furthermore, the reduced surface wind speed happens when there are changes of temperature, geopotential height, and wind speed in the troposphere as well as in the lower stratosphere. All these changes cannot be explained as a local response to the decreasing trend in SH. Most likely, they are linked to the global climate changes.

Some key issues still remain unresolved. For example, why does the $T_s$ have opposite trends during 1960–2003 and 1980–2003 while $T_a$ remains in an increasing trend? How can we distinguish the contribution by the change in local greenhouse gases from that by global atmospheric circulation shift due to the enhanced greenhouse effect globally? More importantly, the surface sensible heating over the TP can generate a strong air pump and regulate the Asian monsoon. Recent studies have reported that the Asian monsoon circulation has been weakened during the past decades (Wang et al. 2004; Xu et al. 2006). To what extent the weakening of the SH over the TP may affect the suppressed Asian monsoon remains unknown. To answer these questions, in particular to understand the influence of the changes in heat source over the TP on the Asian summer monsoon at decadal time scales, a numerical modeling study is imperative. The numerical results will be presented in a separate paper.

*Acknowledgments.* The author thanks Drs. Buwen Dong and Yongsheng Zhang for their valuable suggestions and Dr. Yonghui Weng at the CMA for kindly providing observational data. Thanks are also extended to the anonymous reviewers for their constructive comments on an earlier manuscript. Mr. Shiming Huang helped to process the ISCCP data. This work was supported jointly by the Chinese Ministry of Science and Technology under Grant 2006CB403607, and the Chinese National Science Foundation under Grants 40221503, 40405016, 40475027, and 40523001.

## APPENDIX

### Information of Meteorological Stations over the TP

List of the 71 stations used above 2000 m above mean sea level (MSL), including the station identification number (ID), station name, first year of surface record, latitude (Lat), longitude (Lon), and elevation MSL. Superscript asterisks denote the 12 radiosonde stations in the TP area.

| Number | Station ID | Station name | First year | Lat, North | Lon, East | Elevation (m) |
|---|---|---|---|---|---|---|
| 1 | 51886* | Mangai | 1958 | 38°15′ | 90°51′ | 2945 |
| 2 | 52602 | Lenghu | 1956 | 38°45′ | 93°20′ | 2770 |
| 3 | 52633 | Tuole | 1956 | 38°48′ | 98°25′ | 3367 |
| 4 | 52645 | Yeniugou | 1959 | 38°25′ | 99°35′ | 3320 |
| 5 | 52657 | Qilian | 1956 | 38°11′ | 100°15′ | 2787 |
| 6 | 52707 | Xaozaoho | 1960 | 36°48′ | 93°41′ | 2767 |
| 7 | 52713 | Dachaidan | 1956 | 37°51′ | 95°22′ | 3173 |
| 8 | 52737 | Delingha | 1955 | 37°22′ | 97°22′ | 2982 |
| 9 | 52754 | Gangcha | 1957 | 37°20′ | 100°08′ | 3302 |
| 10 | 52765 | Menyuan | 1956 | 37°23′ | 101°37′ | 2851 |
| 11 | 52787 | Wushaoling | 1951 | 37°12′ | 102°52′ | 3045 |
| 12 | 52818 | Geermu | 1955 | 36°25′ | 94°54′ | 2808 |
| 13 | 52825 | Nuomuhong | 1956 | 36°26′ | 96°25′ | 2790 |
| 14 | 52836* | Dulan | 1954 | 36°18′ | 98°06′ | 3191 |
| 15 | 52856 | Qiaboqia | 1953 | 36°16′ | 100°37′ | 2835 |
| 16 | 52866* | Xining | 1954 | 36°43′ | 101°45′ | 2295 |
| 17 | 52868 | Guide | 1956 | 36°02′ | 101°26′ | 2237 |
| 18 | 52908 | Wudaoliang | 1956 | 35°13′ | 93°05′ | 4612 |
| 19 | 52943 | Xinghai | 1960 | 35°35′ | 99°59′ | 3323 |
| 20 | 55279 | Bange | 1956 | 31°23′ | 90°01′ | 4700 |
| 21 | 55299* | Naqu | 1954 | 31°29′ | 92°04′ | 4507 |
| 22 | 55472 | Shenzha | 1960 | 30°57′ | 88°38′ | 4672 |
| 23 | 55578 | Rikeze | 1955 | 29°15′ | 88°53′ | 3836 |
| 24 | 55591* | Lhasa | 1955 | 29°40′ | 91°08′ | 3649 |
| 25 | 55598 | Zedang | 1956 | 29°15′ | 91°46′ | 3552 |
| 26 | 55664* | Dingri | 1959 | 28°38′ | 87°05′ | 4300 |
| 27 | 55680 | Jiangzi | 1956 | 28°55′ | 89°36′ | 4040 |
| 28 | 55696 | Longzi | 1959 | 28°25′ | 92°28′ | 3860 |
| 29 | 55773 | Pali | 1956 | 27°44′ | 89°05′ | 4300 |
| 30 | 56004* | Tuotuohe | 1956 | 34°13′ | 92°26′ | 4533 |
| 31 | 56018 | Zaduo | 1956 | 32°54′ | 95°18′ | 4066 |
| 32 | 56021 | Qumalai | 1956 | 34°08′ | 95°47′ | 4175 |
| 33 | 56029* | Yushu | 1951 | 33°01′ | 97°01′ | 3681 |
| 34 | 56033 | Maduo | 1953 | 34°55′ | 98°13′ | 4272 |
| 35 | 56034 | Qingshuihe | 1956 | 33°48′ | 97°08′ | 4415 |
| 36 | 56038 | Shiqu | 1960 | 32°59′ | 98°06′ | 4200 |
| 37 | 56046* | Dari | 1956 | 33°45′ | 99°39′ | 3968 |
| 38 | 56067 | Jiuzhi | 1958 | 33°26′ | 101°29′ | 3629 |
| 39 | 56079 | Ruoergai | 1957 | 33°35′ | 102°58′ | 3440 |
| 40 | 56080 | Hezuo | 1957 | 35°00′ | 102°54′ | 2910 |
| 41 | 56093 | Mingxian | 1951 | 34°26′ | 104°01′ | 2315 |
| 42 | 56106 | Suoxian | 1956 | 31°53′ | 93°47′ | 4023 |
| 43 | 56116 | Dingqing | 1954 | 31°25′ | 95°36′ | 3873 |
| 44 | 56125 | Nangqian | 1956 | 32°12′ | 96°29′ | 3644 |
| 45 | 56137 | Changdu | 1954 | 31°09′ | 97°10′ | 3306 |
| 46 | 56144 | Dege | 1956 | 31°48′ | 98°35′ | 3184 |
| 47 | 56146* | Ganzi | 1951 | 31°37′ | 100°00′ | 3394 |
| 48 | 56152 | Seda | 1961 | 32°17′ | 100°20′ | 3894 |
| 49 | 56167 | Daofu | 1957 | 30°59′ | 101°07′ | 2957 |
| 50 | 56172 | Maerkang | 1954 | 30°59′ | 102°14′ | 2664 |
| 51 | 56173 | Hongyuan | 1960 | 32°48′ | 102°33′ | 3492 |
| 52 | 56178 | Xiaojing | 1951 | 31°00′ | 102°21′ | 2369 |
| 53 | 56182 | Songpan | 1951 | 32°39′ | 103°34′ | 2851 |
| 54 | 56202 | Jiali | 1954 | 30°40′ | 93°17′ | 4489 |
| 55 | 56227 | Bomi | 1955 | 29°52′ | 95°46′ | 3736 |
| 56 | 56247 | Batang | 1952 | 30°00′ | 99°06′ | 2589 |
| 57 | 56251 | Xinlong | 1959 | 30°56′ | 100°19′ | 3000 |

| Number | Station ID | Station name | First year | Lat, North | Lon, East | Elevation (m) |
|---|---|---|---|---|---|---|
| 58 | 56257 | Litang | 1952 | 30°00′ | 100°16′ | 3949 |
| 59 | 56312* | Linzhi | 1954 | 29°40′ | 97°50′ | 2990 |
| 60 | 56357 | Daocheng | 1957 | 29°03′ | 100°18′ | 3728 |
| 61 | 56374 | Kangding | 1951 | 30°03′ | 101°58′ | 2616 |
| 62 | 56385 | Emeishan | 1951 | 29°31′ | 103°20′ | 3047 |
| 63 | 56444 | Deqing | 1953 | 28°29′ | 98°55′ | 3319 |
| 64 | 56459 | Muli | 1956 | 27°56′ | 101°16′ | 2427 |
| 65 | 56462 | Jiulong | 1952 | 29°00′ | 101°30′ | 3987 |
| 66 | 56479 | Zhaojue | 1956 | 28°00′ | 102°51′ | 2132 |
| 67 | 56543 | Zhongdian | 1958 | 27°50′ | 99°42′ | 3276 |
| 68 | 56548 | Weixi | 1954 | 27°10′ | 99°17′ | 2326 |
| 69 | 56565 | Yanyuan | 1956 | 27°26′ | 101°31′ | 2545 |
| 70 | 56651 | Lijiang | 1951 | 26°52′ | 100°13′ | 2392 |
| 71 | 56664 | Huaping | 1956 | 26°38′ | 101°16′ | 2245 |

## REFERENCES


Baldwin, M. P., D. W. J. Thompson, E. F. Shuckburgh, W. A. Norton, and N. P. Gillett, 2003: Weather from the stratosphere. *Science,* **301,** 317–319.

Broccoli, A. J., and S. Manabe, 1992: The effects of orography on midlatitude Northern Hemisphere dry climates. *J. Climate,* **5,** 1181–1201.

Chen, B., W. C. Chao, and X. Liu, 2003: Enhanced climate warming in the Tibetan Plateau due to doubling CO2: A model study. *Climate Dyn.,* **2,** 401–413.

Chen, L. X., E. Reiter, and Z. Q. Feng, 1985: The atmospheric heat source over the Tibetan Plateau: May–August 1979. *Mon. Wea. Rev.,* **113,** 1771–1790.

Duan, A. M., and G. X. Wu, 2005: Role of the Tibetan Plateau thermal forcing in the summer climate patterns over subtropical Asia. *Climate Dyn.,* **24,** 793–807.

——, and ——, 2006: Change of cloud amount and the climate warming on the Tibetan Plateau. *Geophys. Res. Lett.,* **33,** L22704, doi:10.1029/2006GL027946.

——, Y. M. Liu, and G. X. Wu, 2005: Heating status of the Tibetan Plateau from April to June and rainfall and atmospheric circulation anomaly over East Asia in midsummer. *Sci. China Ser. D,* **48,** 250–257.

——, G. X. Wu, Q. Zhang, and Y. M. Liu, 2006: New proofs of the recent climate warming over the Tibetan Plateau as a result of the increasing greenhouse gases emissions. *Chin. Sci. Bull.,* **51,** 1396–1400.

Flohn, H., 1957: Large-scale aspects of the summer monsoon in South and East Asia. *J. Meteor. Soc. Japan,* **35,** 180–186.

——, 1960: Recent investigations on the mechanism of the "summer monsoon" of southern and eastern Asia. *Symposium on Monsoons of the World,* Hindu Union Press, 75–88.

Hahn, D. G., and S. Manabe, 1975: The role of mountains in the south Asian monsoon circulation. *J. Atmos. Sci.,* **32,** 1515–1541.

Kitoh, A., 2004: Effects of mountain uplift on East Asian summer climate investigated by a coupled atmosphere–ocean GCM. *J. Climate,* **17,** 783–802.

Li, C. F., and M. Yanai, 1996: The onset and interannual variability of the Asian summer monsoon in relation to land–sea thermal contrast. *J. Climate,* **9,** 358–375.

Li, G., T. Duan, and Y. Gong, 2000: The bulk transfer coefficients and surface fluxes on the western Tibetan Plateau. *Chin. Sci. Bull.,* **45,** 1221–1226.

Li, W. P., G. X. Wu, Y. M. Liu, and Y. Liu, 2001: How the surface processes over the Tibetan Plateau affect the summertime Tibetan Anticyclone: Numerical experiments (in Chinese with English abstract). *Chin. J. Atmos. Sci.,* **25,** 809–816.

Liu, X., and B. Chen, 2000: Climatic warming in the Tibetan Plateau during recent decades. *Int. J. Climatol.,* **20,** 1729–1742.

Luo, H., and M. Yanai, 1983: The large-scale circulation and heat sources over the Tibetan Plateau and surrounding areas during the early summer of 1080. Part I: Precipitation and kinematic analyses. *Mon. Wea. Rev.,* **111,** 922–944.

Niu, T., L. X. Chen, and Z. J. Zhou, 2004: The characteristics of climate change over the Tibetan Plateau in the last 40 years and the detection of climatic jumps. *Adv. Atmos. Sci.,* **21,** 193–203.

Rossow, W. B., and R. A. Schiffer, 1991: ISCCP Cloud Data Products. *Bull. Amer. Meteor. Soc.,* **72,** 2–20.

——, and ——, 1999: Advances in understanding clouds from ISCCP. *Bull. Amer. Meteor. Soc.,* **80,** 2261–2288.

Tao, S.-Y., and Y.-H. Ding, 1981: Observational evidence of the influence of the Qinghai-Xizang (Tibet) Plateau on the occurrence of heavy rain and severe convective storms in China. *Bull. Amer. Meteor. Soc.,* **62,** 23–30.

Wang, Y., and G. Y. Ren, 2005: Change in free atmospheric temperature over China during 1961–2004 (in Chinese with English abstract). *Climatic Environ. Res.,* **10,** 780–790.

Wang, Z., Y. Ding, J. He, and J. Yu, 2004: An updating analysis of the climate changes in China in recent 50 years (in Chinese). *Acta Meteor. Sin.,* **62,** 228–236.

Wu, G. X., and Y. S. Zhang, 1998: Tibetan Plateau forcing and the timing of South Asia monsoon and South China Sea monsoon. *Mon. Wea. Rev.,* **126,** 913–927.

——, and Y. M. Liu, 2000: Thermal adaptation, overshooting, dispersion, and subtropical high. Part I: Thermal adaptation and overshooting (in Chinese with English abstract). *Chin. J. Atmos. Sci.,* **24,** 433–436.

——, W. P. Li, H. Guo, H. Liu, J. S. Xue, and Z. Z. Wang, 1997: Sensible heat driven air-pump over the Tibetan Plateau and its impacts on the Asian Summer Monsoon. *Collections on the Memory of Zhao Jiuzhang,* Y. Duzheng, Ed., Chinese Science Press, 116–126.

——, Y. M. Liu, J. Y. Mao, X. Liu, and W. P. Li, 2004: Adaptation of the atmospheric circulation to thermal forcing over the Tibetan Plateau. *Observation, Theory and Modeling of Atmospheric Variability,* X. Zhu, Ed., World Scientific Press, 92–114.

——, and Coauthors, 2007: Review and new insights in the sensible heat driving air-pump over the Tibetan Plateau and its influence on the climate in Asia. *J. Hydrol.,* **8,** 770–789.

Xu, M., C.-P. Chang, C. Fu, Y. Qi, A. Robock, D. Robinson, and H. Zhang, 2006: Steady decline of east Asian monsoon winds, 1969–2000: Evidence from direct ground measurements of wind speed. *J. Geophys. Res.,* **111,** D24111, doi:10.1029/2006JD007337.

Yanai, M., 1961: A detailed analysis of typhoon formation. *J. Meteor. Soc. Japan,* **39,** 187–214.

——, and C. Li, 1994: Mechanism of heating and the boundary layer over the Tibetan Plateau. *Mon. Wea. Rev.,* **122,** 305–323.

——, and G. X. Wu, 2006: Role of the Tibetan Plateau on Asia monsoon. *The Asian Monsoon,* B. Wang, Ed., Springer, 513–629.

——, C. Li, and Z. Song, 1992: Seasonal heating of the Tibetan

Plateau and its effects on the evolution of the Asian summer monsoon. *J. Meteor. Soc. Japan,* **70,** 319–351.

Yeh, T. C., and Y. X. Gao, 1979. *Meteorology of the Qinghai-Xizang (Tibet) Plateau.* Science Press, 278 pp.

——, and G. X. Wu, 1998: The role of the heat source of the Tibetan Plateau in the general circulation. *Meteor. Atmos. Phys.,* **67,** 181–198.

——, S. W. Lo, and P. C. Chu, 1957: On the heat balance and circulation structure in troposphere over Tibetan Plateau (in Chinese). *Acta Meteor. Sin.,* **28,** 108–121.

Yu, R. C., B. Wang, and T. J. Zhou, 2004: Tropospheric cooling and summer monsoon weakening trend over East Asia. *Geophys. Res. Lett.,* **31,** L22212, doi:10.1029/2004GL021270.

Zhang, Y. S., T. Li, and B. Wang, 2004: Decadal change of the spring snow depth over the Tibetan Plateau: The associated circulation and influence on the East Asian summer monsoon. *J. Climate,* **17,** 2780–2793.

Zhao, P., 1999: The heating status over the Tibetan Plateau and its relationship with the air–sea interaction. Ph.D. thesis, Chinese Academy of Meteorological Sciences, Beijing, China, 229 pp.

——, and L. X. Chen, 2001: Climate features of atmospheric heat source/sink over the Qinghai-Xizang Plateau in 35 years and its relation to rainfall in China. *Sci. China Ser. D,* **44,** 858–864.

Zhou, M. Y., and Coauthors, 2000: *Observation in the Atmospheric Boundary Layer and Investigation of Dynamic Meteorology over the Tibetan Plateau.* Meteorology Press, 125 pp.

Zhou, S., and R. Zhang, 2005: Decadal variations of temperature and geopotential height over the Tibetan Plateau and their relations with Tibet ozone depletion. *Geophys. Res. Lett.,* **32,** L18705, doi:10.1029/2005GL023496.

Zhu, W., L. Chen, and X. Zhou, 2001: Several characteristics of contemporary climate change in the Tibetan Plateau. *Sci. China Ser. D,* **44** (Suppl.), 410–420.